Supplementary Materials: Fluorescence and Physico-Chemical Properties of Hydrogenated Detonation Nanodiamonds

Giannis Thalassinos [1], Alastair Stacey [1], Nikolai Dontschuk [2], Billy J. Murdoch [3], Edwin Mayes [3], Hugues A. Girard [4], Ibrahim M. Abdullahi [5], Lars Thomsen [6], Anton Tadich [6], Jean-Charles Arnault [4], Vadym N. Mochalin [5], Brant C. Gibson [1], and Philipp Reineck [1],

1. Electron-energy loss spectrum (EELS)

Example of C1s K-edge EELS spectra of DND-H Anneal and DND-H Plasma used to determine the sp^2/sp^3 ratio for each pixel in Figure 2 C & D.

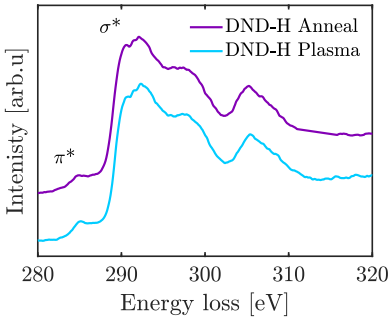

Figure S1. Electron-energy loss spectra of the C1s K-edge for DND-H Anneal and DND-H Plasma samples.

2. Near-edge X-ray absorption fine structure (NEXAFS)

The sp^2 content was determined using the expression

$$sp^2(\%) = \frac{I_s^{\pi*}}{I_s^{\sigma}} \times \frac{I_{HOPG}^{\sigma}}{I_{HOPG}^{\pi*}} \times 100, \quad (1)$$

where I represents the integrals of the areas between 283.0–285.5 eV (π*) and 289.0–320.0 eV (σ) in both the sample (s) and the highly oriented pyrolytic graphite ($HOPG$) reference. See Figure S2 for visual representation of these ranges.

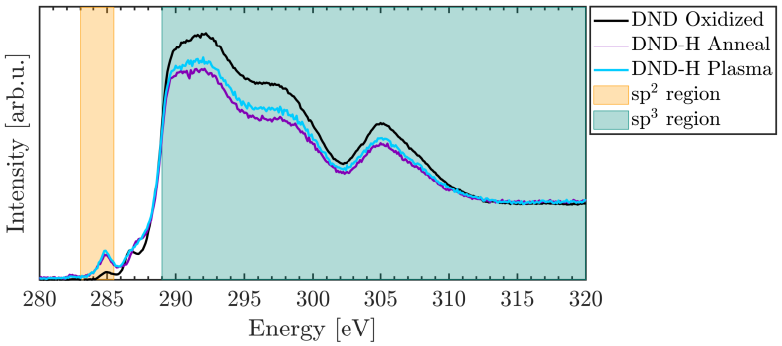

Figure S2. Carbon K-edge NEXAFS spectra with shaded sp^2 and sp^3 ranges used for determining the sp^2/sp^3 ratio.

3. X-ray photoelectron spectroscopy (XPS)

Both DND-H Anneal and DND-H Plasma experienced mild charging of 2.0 eV. DND Oxidized had higher levels of charging of 13.0 eV consistent with differences in electrical conductivity between

hydrogenated and oxidized DNDs. Figure S3 shows raw data not corrected for this charging. The two pairs of peaks found at approximately 85 eV and 350 eV originate from the Au-coated substrate.

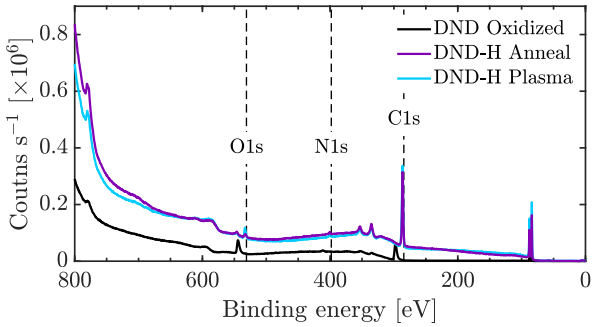

Figure S3. Full XPS spectra of the starting oxidized DND and both hydrogenated DND samples. Spectra not corrected for charging effects.

4. Fourier-Transform infrared (FTIR) spectroscopy

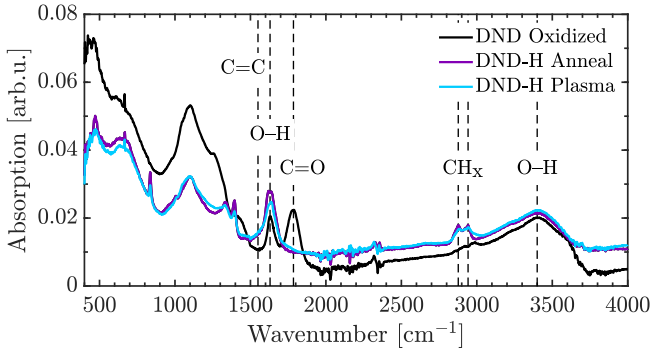

Figure S4. Full range of FTIR data for the starting DND Oxidized material and the two hydrogenated DND samples.

5. Colloidal properties

5.1. Averages of DLS and ζ-potential

Averages of the aggregate diameters and ζ-potentials of both hydrogenated DND samples.

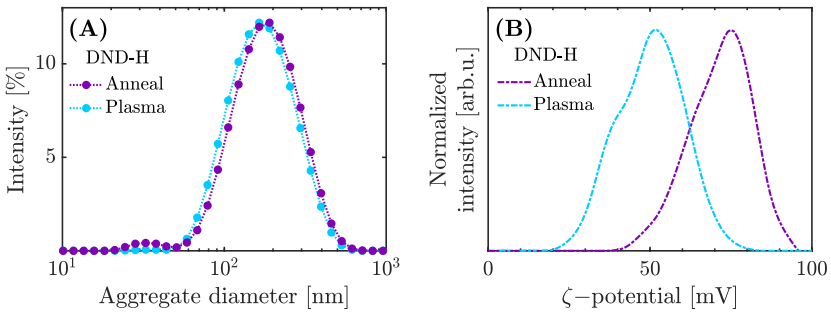

Figure S5. Colloidal properties of hydrogenated DND particles dispersed in water at ∼0.4 mg mL^{-1}. **(A)** The averaged intensity-weighted size distribution of the DND aggregates, and **(B)** their corresponding averaged ζ-potential.

5.2. Dynamic light scattering (DLS)

Raw DLS data showing intensity, numeric, and volumetric weighted distributions of aggregate diameters for both DND-H Anneal and DND-H Plasma samples. Intensity weighted data shows peaks

mainly around ∼180 nm. Number weighted data indicates a large population of smaller aggregates on the order of 20 nm in diameter. These smaller aggregates however are less frequently detected in DND-H Plasma.

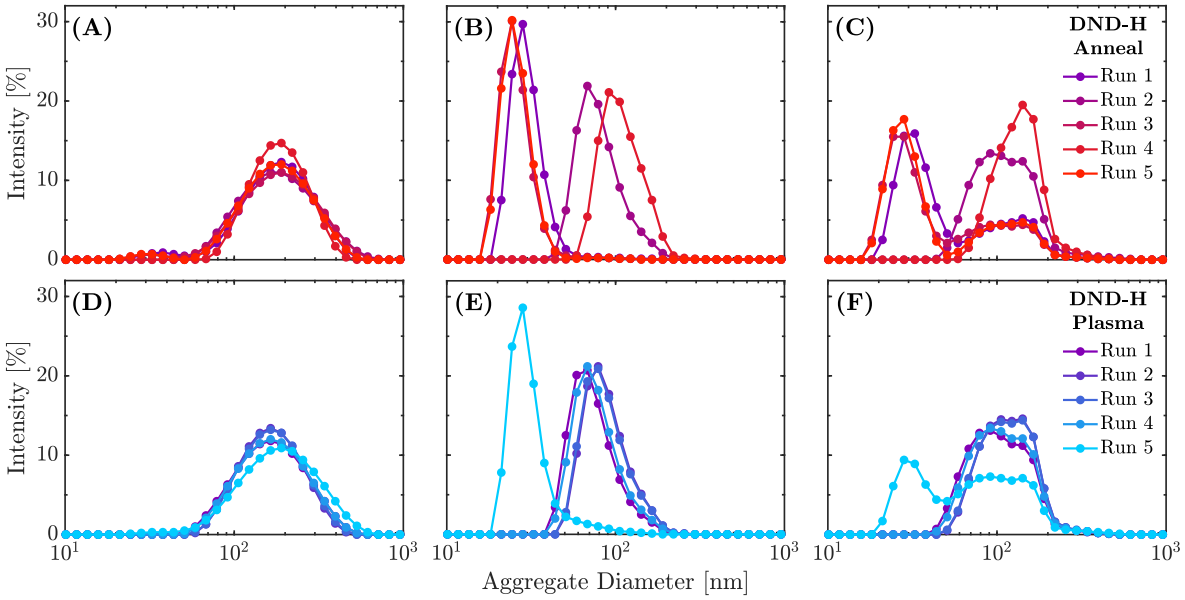

Figure S6. Raw dynamic light scattering results for both **(A–C)** DND-H Anneal and **(D–F)** DND-H Plasma samples with **(A & D)** intensity; **(B & E)** number; and **(C & F)** volume weighted distributions.

5.3. Zeta-potential

Zeta-potential and DLS measurements were taken on order of months after hydrogenation in the case of both materials. Therefore, temporal effects on the ζ-potential were not examined throughout this study. Raw ζ-potential data (Figure S7) shows a wide but relatively consistent distribution for both samples, with the exception of a couple outliers. DND-H Anneal has a consistently higher ζ-potential compared to the DND-H Plasma sample.

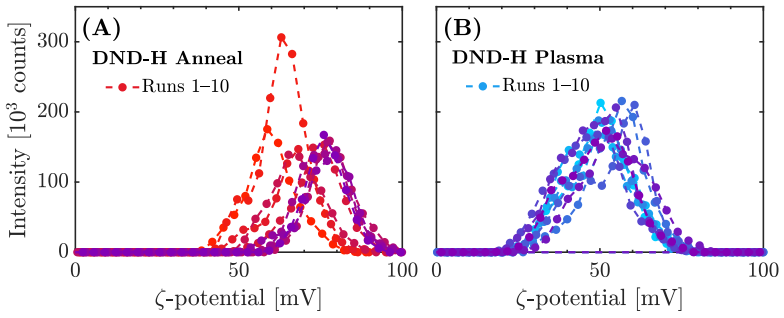

Figure S7. Raw ζ-potential for **(A)** DND-H Anneal and **(B)** DND-H Plasma samples.

6. In-solution spectra

In-solution spectra of both DND-H Anneal and DND-H Plasma suspended in deionized (DI) water (both ∼0.4 mg mL^{-1}) were obtained using our custom-built setup (see Figure S8) for excitation wavelengths λ_{ex} ranging from 400–600 nm with excitation powers and accompanying filters shown in Table S1.

Raw fluorescence spectra for each λ_{ex} are presented in Figure S9 D & E with a pure DI water reference in Figure S9F. The final spectra shown in Figure S9 A & B were derived by subtracting the water signals from each spectra and normalizing for differences in excitation power to 6.4 mW.

Differences in brightness between each λ_{ex} were determined by integrating the area under each curve from 660–800 nm to analyse only the spectral region in which the data was collected for each condition.

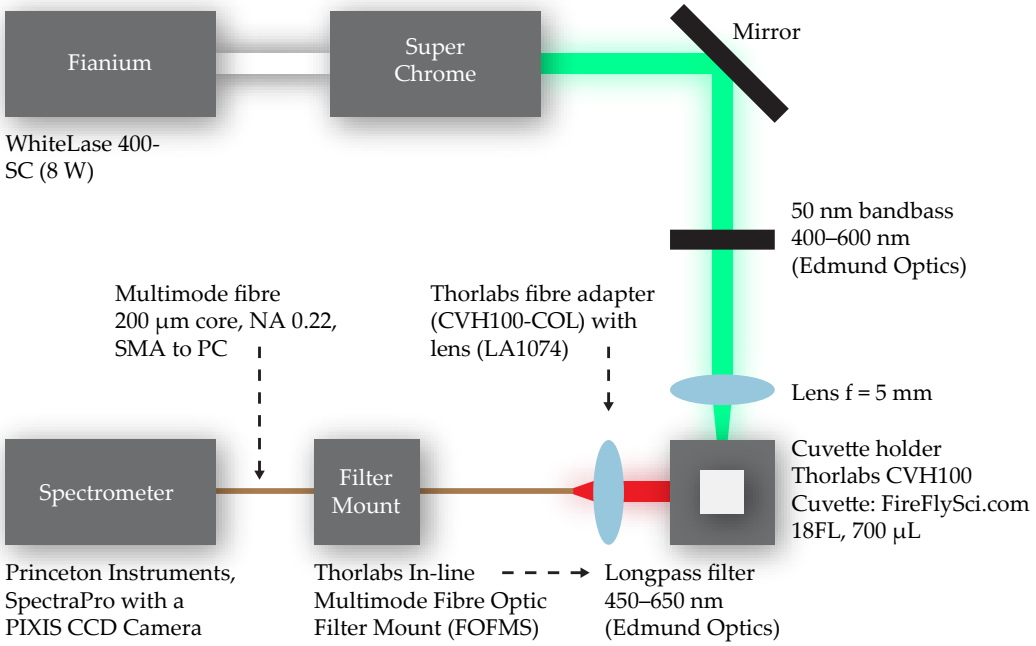

Figure S8. Schematic of our custom-built in-solution spectroscopy setup used for all in-solution experiments with all components labelled.

Table S1. Combination of excitation wavelength, power, and filters used for in-solution fluorescence spectroscopy measurements. Total acquisition time for each spectrum was 100 s. Excitation laser source was set to 80 MHz repetition rate for all excitation conditions.

Excitation wavelength [nm]	Filters (Band/Long Pass) [nm]	Excitation power [mW]
400 ± 20	400/450	6.2
450 ± 20	450/500	6.6
500 ± 20	500/550	6.4
550 ± 20	550/600	6.3
600 ± 20	600/650	6.7

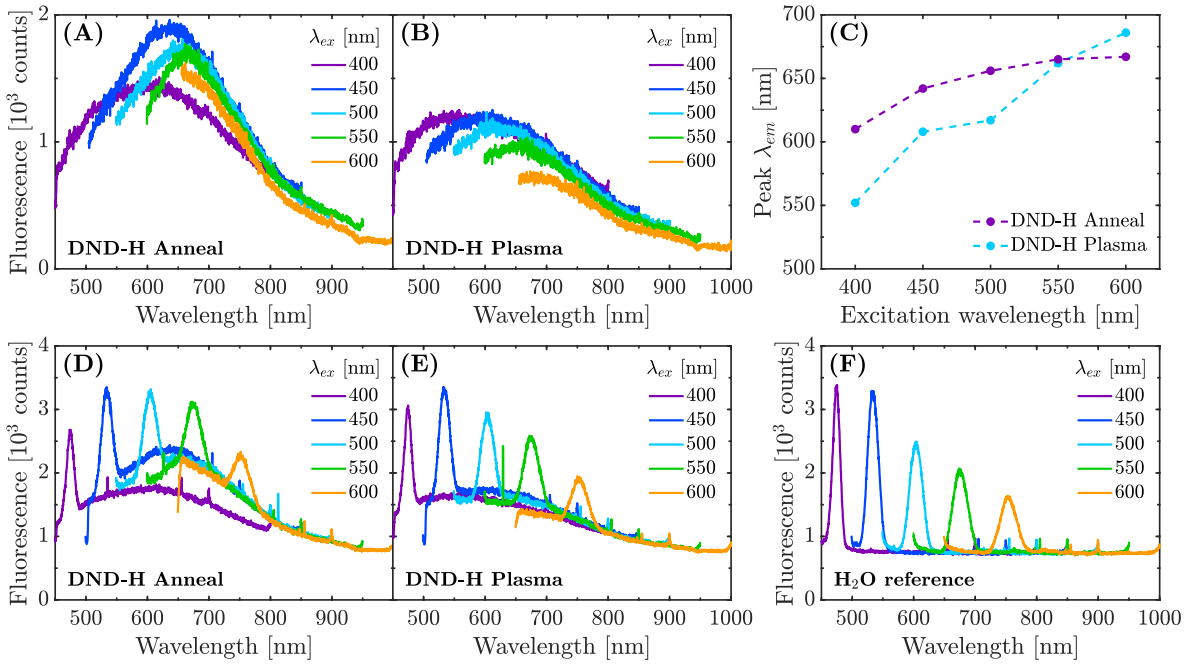

Figure S9. In-solution spectra of **(A)** DND-H Anneal and **(B)** DND-H Plasma samples at different excitation wavelengths; normalized for differences in excitation power. **(C)** Change in peak emission wavelength as a function of excitation wavelength. Raw **(D)** DND-H Anneal and **(E)** DND-H Plasma results not corrected for differences in excitation power or **(F)** water signal.

7. Room-temperature spectra

Photoluminescence (PL) maps of both hydrogenated DND samples drop cast onto ∼5×5 mm Si wafers in a dried state. DND-H Anneal sample generally exhibits less aggregation compared to the DND-H Plasma sample. Average spectral properties were very similar between the two materials, though variations were often present. Some artefacts remain in the individual spectra in Figure S11 and are represented as sharp spikes.

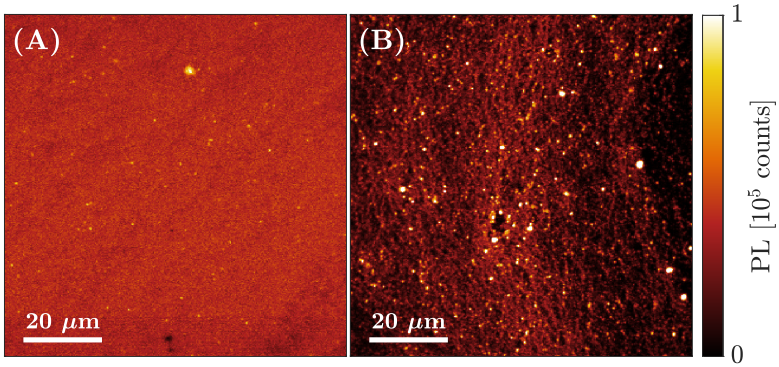

Figure S10. Room-temperature solid state PL maps of **(A)** DND-H Anneal and **(B)** DND-H Plasma samples drop-cast onto Si wafers. Excited using a 532 ± 30 nm pulsed excitation source at 5 MHz repetition rate at 50 µW.

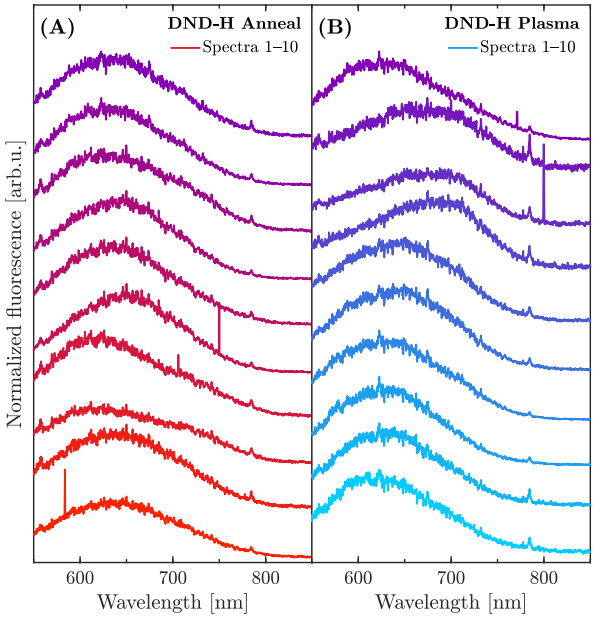

Figure S11. Room-temperature solid state fluorescence spectra of **(A)** DND-H Anneal and **(B)** DND-H Plasma samples corresponding to PL maps in Figure S10.

8. Temperature-dependence experiments

Cryogenic measurements were performed by simultaneously placing both DND-H samples inside the Cryostation and taking measurements starting from room temperature in ambient air, down towards 10 K in vacuum. Each curve in Figure S12 is the averaged, normalized spectrum from 10 individual spots, each of which is comprised of 10× 10 s individual spectra (i.e. 100 s total acquisition time per spot over 10 spots). The faded envelopes around the solid curves represent the standard deviation for each spectrum. Some artefacts remain where background removal was unsuccessful. These appear as either upward or downward spikes and are usually found in the same locations across all spectra.

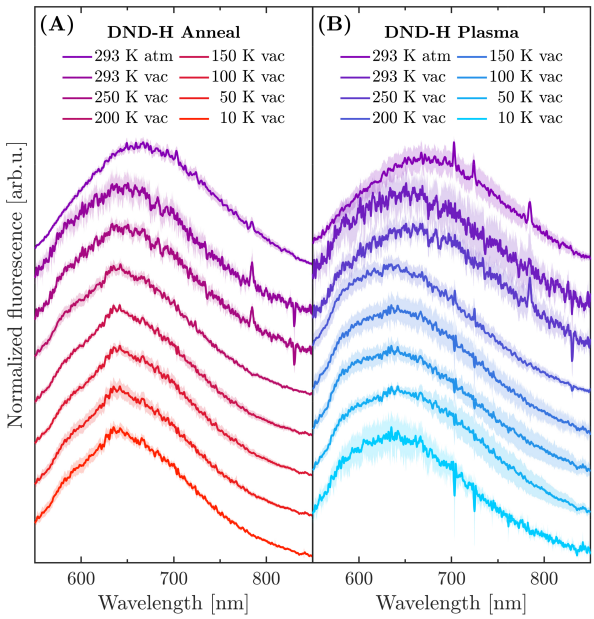

Figure S12. Averaged fluorescence spectra of **(A)** DND-H Anneal and **(B)** DND-H Plasma samples for temperatures ranging from 293 K in air atmosphere and vacuum to 10 K. Faded envelopes around solid lines indicate standard deviation between measurements.

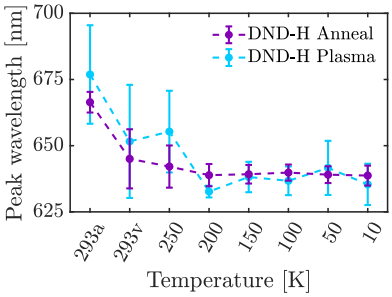

Figure S13. Peak emission wavelength of hydrogenated DND samples on Si substrates as a function of changing temperature. Postscripts 'a' and 'v' refer to ambient atmospheric pressure and in-vacuum respectively. All measurements at temperatures <293 K were performed in vacuum.